RESEARCH ARTICLE

Afforestation on cropland promotes pedogenic inorganic carbon accumulation in deep soil layers on the Chinese loess plateau

Jiabin Liu · Puxia Wu · Zhong Zhao · Yang Gao

Abstract

Aims Over the past decades, vast croplands have been converted into forestland on the Chinese Loess Plateau (CLP). Although a few studies have investigated the effects of afforestation on soil inorganic carbon (SIC), there has been little information on the changes in the two fractions of SIC, pedogenic inorganic carbon (PIC) and lithogenic inorganic carbon (LIC), along a deep profile following afforestation.

Methods We selected forestland (*Robinia pseudoacacia*; 31 years) and adjacent cropland (control), and investigated the stocks of SIC, PIC and LIC, at 0-300 cm under the two lands on the CLP.

Results The SIC stock significantly decreased by 60.2 Mg ha^{-1} at 0-80 cm but increased by 57.8 Mg ha^{-1} at 80-220 cm, and no significant difference in total SIC stock at 0-300 cm was observed between the two lands. Afforestation significantly reduced the LIC stock in each layer; afforestation decreased the PIC stock at 0-80 cm but elevated it at 80-300 cm. In the 80-220 cm layer of forestland, the LIC stock decreased by 41.1 Mg ha^{-1} while the PIC stock increased by 98.9 Mg ha^{-1}.

Conclusions Afforestation on cropland induces the loss of SIC in upper layers. However, it promotes the accumulation of PIC in deep layers, which causes an increase of SIC in these layers. Because the net increased PIC in deep layers compensates for the loss of SIC in the upper layers, afforestation on cropland does not alter the total SIC storage but redistributes the SIC along the profile on the CLP.

Keywords Soil inorganic carbon · Pedogenic inorganic carbon · Lithogenic inorganic carbon · Forestland · Cropland

Responsible Editor: Katharina Maria Keiblinger.

J. Liu · Z. Zhao · Y. Gao (✉)
College of Forestry, Northwest A&F University, No.3 Taicheng Road, Yangling 712100, Shaanxi, China
e-mail: gaoyang0912@nwafu.edu.cn

J. Liu
College of Natural Resources and Environment, Northwest A&F University, Yangling 712100, Shaanxi, China

P. Wu
Key Laboratory of State Forestry Administration on Soil and Water Conservation & Ecological Restoration of Loess Plateau, Shannxi Academy of Forestry, Xi'an 710082, Shannxi, China

Introduction

The soil carbon pool accounts for more than twice the amount of carbon in the vegetation or the atmosphere (Lal 2004; Schmidt et al. 2011). Even a subtle fluctuation of such a tremendous carbon pool could potentially disturb the global carbon budget, and soil carbon dynamics are essential for predicting the future global climate (Belay-Tedla et al. 2009; Tamir et al. 2012). Mounting evidence shows that afforestation has great potential to alter soil carbon pools, and the

effects of afforestation on soil carbon have received considerable attention (Jackson et al. 2002). The soil carbon pool is composed of the soil organic carbon (SOC) pool and the soil inorganic carbon (SIC) pool (Lal 2009). The SIC storage at 0-200 cm can be approximately ten or even up to seventeen times larger than the SOC storage in dry lands (Schlesinger 1982; Emmerich 2003; Mi et al. 2008; Zamanian et al. 2016). Due to the amount of SIC far exceeding SOC in semiarid areas, a minor variation in the SIC pool following afforestation could play a more efficient role than a major fluctuation in the SOC pool in terms of altering the regional carbon budget (Wang et al. 2016; Gao et al. 2017; An et al. 2019; Ferdush and Paul 2021). Therefore, change in the SIC pool following afforestation in semiarid regions needs to be thoroughly understood.

Furthermore, the SIC pool can be subdivided into lithogenic and pedogenic inorganic carbon subpools with different $\delta^{13}C$ values (Monger et al. 2015). Lithogenic inorganic carbon (LIC) is inherited from the soil parent material and its $\delta^{13}C$ value is close to zero; pedogenic inorganic carbon (PIC) is formed through the precipitation or reprecipitation of carbonate material, and its $\delta^{13}C$ value is normally negative (Stevenson et al. 2005). The percentages of LIC and PIC in SIC can be differentiated by measuring the $\delta^{13}C$ values of SIC and SOC ($\delta^{13}C$-SIC and $\delta^{13}C$-SOC) (Landi et al. 2003; Wang et al. 2014; Bughio et al. 2016; Gao et al. 2018). The changes in LIC and PIC along the profile following land use change can clearly reflect the dissolution and precipitation of SIC (Rao et al. 2006; Monger et al. 2015; Zamanian et al. 2016; Xiao et al. 2020). However, most of the present studies only inferred or estimated the rough dynamics of PIC following afforestation in drylands (Chang et al. 2012; Jin et al. 2014; Wang et al. 2016; Gao et al. 2017), and few studies have focused on the exact changes in LIC and PIC stocks, particularly on the Chinese Loess Plateau (CLP).

The CLP is a unique geographical unit in semiarid region and is characterized by a high carbonate content. The SIC content in the deep (> 40 cm) layers in this region is at least three times higher than the SOC content, and the mean SIC density (22.3 kg C m^{-3}) is approximately two times higher than the national average (Mi et al. 2008; Wu et al. 2009). On the CLP, numerous croplands suffered from soil degradation and low yields as a result of long-term intensive tillage (He et al. 2016). To protect soil and improve the local ecological environment, vast croplands have been converted into forestland over the past decades, which significantly alters the soil carbon pool on the CLP (Deng et al. 2014). It is known that afforestation on cropland induces SOC sequestration by introducing substantial organic matter into the soil (Deng et al. 2014; Yang et al. 2021), and a few studies have investigated the distributions of SIC stock along the profile under cropland and forestland on the CLP (Han et al. 2018; Zhang et al. 2015; Yu et al. 2020; Song et al. 2020). However, there has been little information on the changes in PIC and LIC stocks following afforestation, and this information could offer a better understanding of the mechanism on the variation in SIC following afforestation.

In the present study, we selected forestland (*Robinia pseudoacacia*; 31 years) and adjacent cropland (control) with the same topographical and geological backgrounds, measured the SIC contents, $\delta^{13}C$-SOC and $\delta^{13}C$-SIC, and calculated the stocks of SIC, PIC and LIC at 0-300 cm under the two lands on the CLP. The objectives were to (a) investigate the changes in the stocks of SIC, PIC and LIC along the profile of 0-300 cm after afforestation on cropland and (b) discuss the potential reasons for the variation in SIC based on the changes in PIC and LIC following afforestation.

Materials and methods

Study site

The study site is located in Huaiping Farm, Yongshou County, Shannxi Province, China (34°80-34°82′ N, 108°15-108°18′E). The region has a typical semiarid continental climate. The mean annual temperature and precipitation are 12.1 °C and 576 mm, respectively. The elevation is 1123 m. The soil is a dark loessial soil, and is classified as Calcaric Cambisols (World Reference Base for Soil Resources 2014) with a clay content of 19.6% and a silt content of 61.3%.

At the study site, a pair of neighbouring cropland and forestland was selected (Fig. 1). Before 1987, the topographical and geological backgrounds of the forestland were completely consistent with those of the cropland. The position of the current forestland has been used as cropland until 1987, and the management and history strategy for this land was the
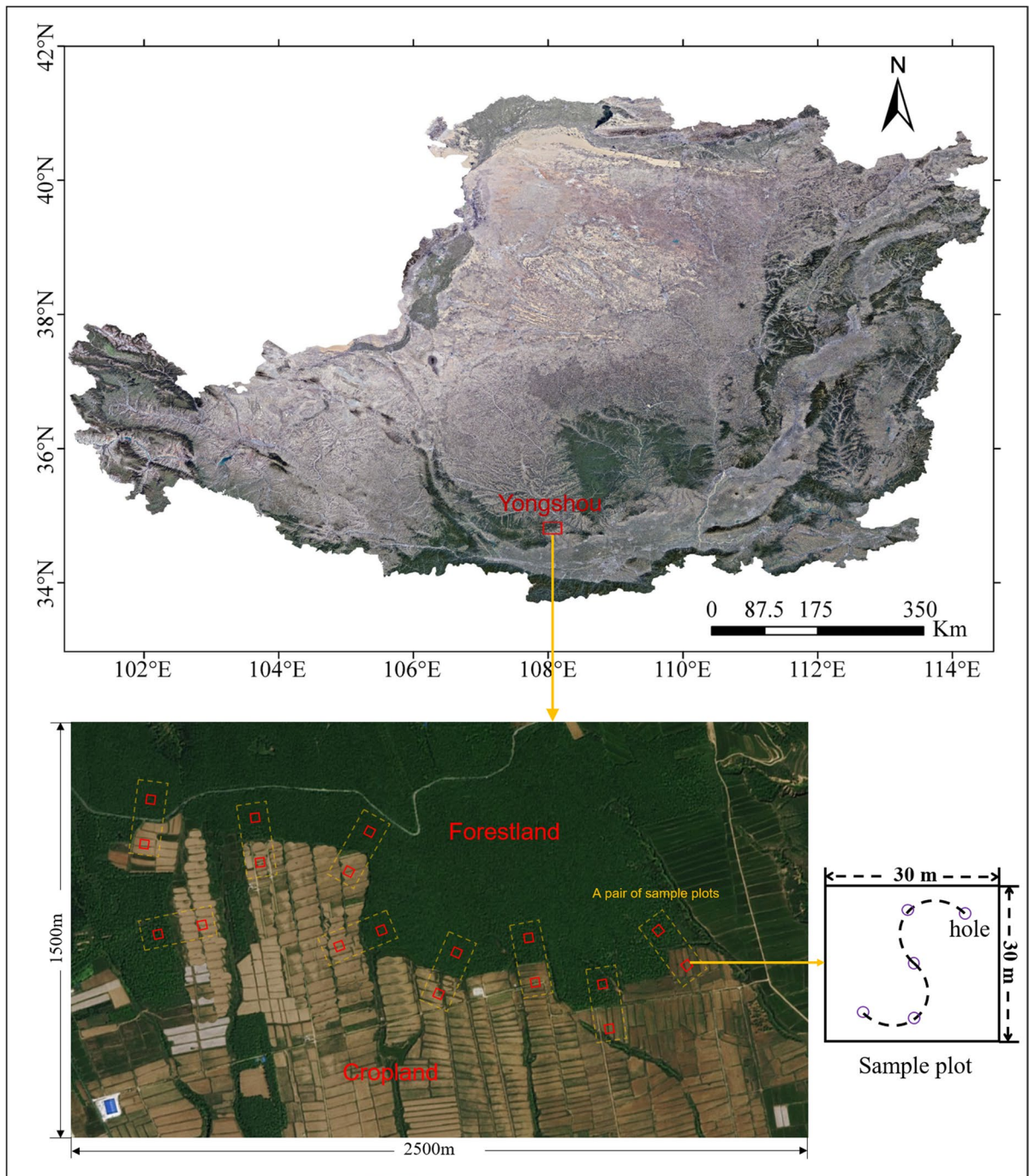
Fig. 1 Location of the study site and the distribution of the sample plots in the study site

same as that for the current cropland before afforestation. In 1987, *R. pseudoacacia* was directly planted in the cropland by seedling. After the implementation of the tree plantation, there was little human activity

in the forestland. Since afforestation, no fertilization has been conducted in the forestland. The groundwater level at the study site (at least >30 m) is far below the investigative rhizosphere, and no river is found at

the study site. When rainstorm occurred, the direction of overland runoff was roughly from west to east. The whole study site is a rain-fed land, and no irrigation was conducted in the two lands during any period. *Triticum aestivum-Solanum tuberosum* or *T. aestivum-Fagopyrum esculentum* was rotationally cultivated in the cropland. When the crops were planted, $CO(NH_2)_2$ was the only fertilizer used, with an annual input of 140-210 kg N ha^{-1}.

Soil sampling

In April 2018, one forestland (treatment) and its adjacent cropland (control) were selected within a large and flat area (scope of 1.5 km × 2.5 km) in the study site. On each land, nine sample plots (30 m × 30 m for each plot) were selected along the boundary. To ensure that the topographical and geological backgrounds between the treatment and the control were consistent, two adjacent sample plots on both sides of the boundary were set up as a pair, and 9 pairs of sample plots along the boundary were selected in the study site. All the sampling plots were at least 50 m away from the boundary to reduce the effects of forestland on cropland, and two neighbouring pairs were at least 150 m apart. The distribution of the sample plots is shown in Fig. 1. In each sample plot of forestland, nine live trees were randomly selected to measure the height and diameter at breast height (DBH). The mean height and DBH were 14.4 m and 16.7 cm, respectively. The tree density and canopy coverage in the forestland were 1187 tree ha^{-1} and 78%, respectively. In each sample plot, five holes (300 cm deep) were drilled by a soil auger (5 cm diameter) along an S-shaped curve to obtain the soil sample (Fig. 1). When drilling, all the litter was removed and the interval was set as 20 cm. The 5 soil samples collected from the same layer in each sample plot were completely mixed into a composite sample (approximately 500 g). After all 270 composite samples (18 sample plots × 15 composite samples per sample plot) were air dried, all roots were picked out. All samples were fully ground using an agate mortar, passed through a 0.1 mm sieve and prepared for the measurements of the total soil carbon (TSC) content, SOC content and the values of δ^{13}C-SIC and δ^{13}C-SOC. Within each sample plot, a soil profile at a depth of 300 cm was excavated. For each profile, 15 metal cores (100 cm^3 for each core) were driven into

the soil at an interval of 20 cm. All the soil cores were dried at 105 °C for 48 h and were weighed to measure the soil bulk densities.

From May to October 2018, the soil water content (SWC) and soil CO_2 concentration under the two lands were measured when heavy rain (rainfall intensity >25 mm day^{-1}) occurred. Forty-eight hours after each heavy rain event, 3 holes (300 cm deep) in each sample plot were drilled by a soil auger at the interval of 20 cm to obtain soil sample, and the soil samples were weighted and dried at 105 °C for 24 h to measure the SWC. After the soil sampling, a soil gas sampler (DIK-5520-13; Daiki Rika Kogyo, Saitama, Japan) was inserted into the soil at 50 cm depth within each sample plot and 150 mL gas sample was extracted. The obtained gas was injected into an LI-840A (LI-COR Environmental, Lincoln, NE, USA) to measure the soil CO_2 concentration. During this period, heavy rain occurred 5 times.

Soil analyses

The SOC contents and TSC contents of all 270 sieved samples were determined using the dichromate oxidation procedure (Walkley and Black 1934) and the Vario EL III elemental analyzer (Elementar, Germany), respectively. The SIC contents were obtained by subtracting the SOC contents from TSC contents, which was specified in Wang et al. (2012). To determine δ^{13}C-SOC for each sieved sample, 5 g of soil was steeped in excessive HCl (2 mol L^{-1}) for 24 h for eliminating the SIC. Twenty-four hours later, the acidified soil was repetitiously washed with distilled water until its pH exceeded 5, and then the washed soil was dried at 40 °C. Approximately 30 mg of dried soil was combusted at 1000 °C in an elemental analyzer (EA; Flash EA 1112) for converting the SOC into CO_2. The generated CO_2 was transported into an isotope ratio mass spectrometer (IRMS; Finnigan MAT Delta plus XP) for measuring δ^{13}C-SOC value. Each sample was measured in triplicate, and the standard deviation of the reported δ^{13}C-SOC among the three measurements was within 0.3 ‰. To determine the δ^{13}C-SIC for each sieved sample, approximately 100 mg of soil was fully reacted with 5 mL of pure H_3PO_4 at 75 °C for 4 hours in a 12 mL sealed vessel of Gas Bench II (Thermo Fisher Scientific, Inc.) for converting the SIC into CO_2. The generated CO_2 was transported into the IRMS for

measuring δ^{13}C-SIC value. Each sample was measured in triplicate, and the standard deviation of the reported δ^{13}C-SIC among the three measurements was within 0.3 ‰.

Calculations of SIC, PIC and LIC stocks and statistical analyses

On the basis of Landi et al. (2003), Ryskov et al. (2008) and Wang et al. (2014), the PIC content was calculated as follows:

$$PIC \text{ content} = \frac{\delta^{13}C\text{-}SIC - \delta^{13}C\text{-}LIC}{\delta^{13}C\text{-}PIC - \delta^{13}C\text{-}LIC} \times SIC \text{ content} \quad (1)$$

Where δ^{13}C-SIC, δ^{13}C-LIC and δ^{13}C-PIC are the δ^{13}C values of bulk SIC, LIC and PIC, respectively. According to the results of Liu et al. (2011) and Wang et al. (2014) on the CLP, the δ^{13}C-LIC in this study was set as −1‰. The δ^{13}C-PIC was calculated as described in Mermut et al. (2000), Landi et al. (2003) and Ryskov et al. (2008):

$$\delta^{13}C\text{-}PIC = \delta^{13}C\text{-}SOC + 14.9‰ \quad (2)$$

where the value of 14.9, including the isotopic fractionation of 10.5 for carbonate precipitation and 4.4 for CO_2 diffusion (Cerling et al. 1989, 1991), represents the mean difference between δ^{13}C-SOC and δ^{13}C-PIC.

The LIC content was calculated as follows:

$$LIC \text{ content} = SIC \text{ content} - PIC \text{ content} \quad (3)$$

The SIC stock was calculated as follows:

$$M = 0.1 \times D \times B \times Z \times ((100 - G)/100) \quad (4)$$

where M (Mg ha^{-1}) is the soil carbon stock; D (cm) is the soil depth; B (g cm^{-3}) is the soil bulk density; Z (g kg^{-1}) is the soil carbon content; and G (%) is the gravel content, which was 0 in this study. After obtaining the contents of PIC and LIC, the stocks of PIC and LIC were also calculated using Eq. (4).

A paired-samples t-test was performed to examine the significance of the differences in relevant variables between cropland and forestland at the same depth. Multiple-comparisons and a one-way analysis of variance procedures were used to compare the differences in relevant variables among the soil depths for each land. All statistical analyses were conducted

in Matlab software (7.12.0.635, The Mathworks, Natick, MA, USA).

Results

Changes in soil properties, δ^{13}C-SIC and δ^{13}C-SOC values following afforestation

The SIC contents at 0-80 cm were significantly lower under the forestland than under the cropland, while the SIC contents at 80-220 cm under the forestland were significantly higher than the cropland (Fig. 2a). No significant difference in SIC content at 220-300 cm was found between the two lands. The SOC content in each layer under the forestland was significantly higher than that under the cropland (Fig. 2b). The soil pH at 0-160 cm under the forestland were significantly lower than those under the cropland, and no significant difference in soil pH below 160 cm was observed between the two lands (Table 1). Compared to the cropland, the bulk densities under the forestland were significantly lower in the top 80 cm layers, while there was no significant difference in bulk density at 80-300 cm between the two lands (Table 1). When no rainfall was occurring, there was no significant difference in SWC at 0-80 cm between the forestland and cropland, while the SWC below 80 cm under the forestland were much lower than the cropland (Fig. 3a). After rainfall, the SWC at 0-60 cm under the forestland were significantly higher than the cropland, and the SWC at 160-300 cm under the forestland were significantly lower than the cropland (Fig. 3b-f). After rainfall, the soil CO_2 concentration at 50 cm under the forestland was remarkably higher than that under the cropland (Fig. 4).

The forestland showed a significantly lower δ^{13}C-SIC value than the cropland at each soil layer (Fig. 5a), however, no significant difference in δ^{13}C-SOC at each layer was found between the two lands (Fig. 5b). The δ^{13}C-SIC values showed an increasing trend with depth under the cropland. In the forestland, the δ^{13}C-SIC values were significantly lower at 0-180 cm than at 180-300 cm, and no significant difference in δ^{13}C-SIC value was
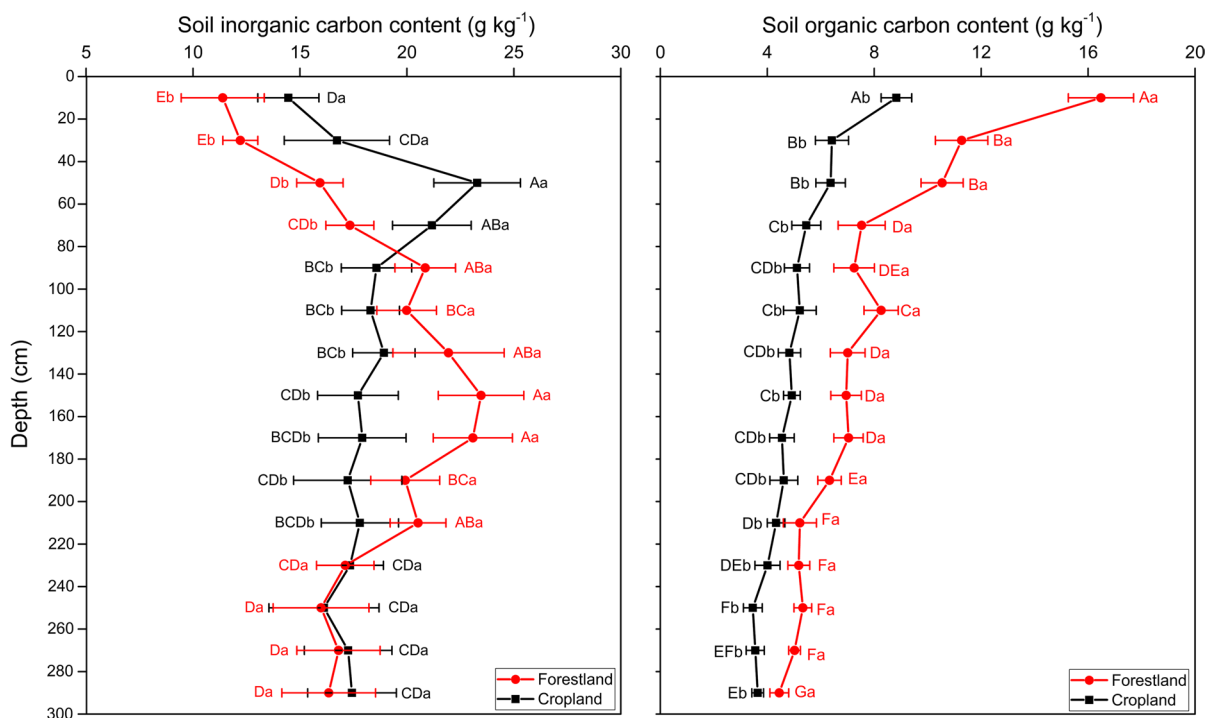
Fig. 2 Soil inorganic carbon and soil organic carbon contents under the forestland and cropland. Within each land-use, different uppercase letters denote significant differences among the depths, and within each depth, different lowercase letters denote significant differences between the land-uses (mean ± standard deviations; n = 9; significance of the difference was considered as $P < 0.05$). In all figures in this study, letters with red color were labeled for forestland, and letters with black color were labeled for cropland

observed among the 0-180 cm layers and among the 220-300 cm layers, respectively (Fig. 5a).

Changes in SIC, PIC and LIC stocks following afforestation

The SIC stocks at 0-300 cm under the cropland and forestland were 643.1 Mg ha^{-1} and 636.2 Mg ha^{-1}, respectively, and no significant difference in total SIC stock was observed between the two lands. After afforestation on cropland, the SIC stock significantly decreased by 60.2 Mg ha^{-1} at 0-80 cm but significantly increased by 57.8 Mg ha^{-1} at 80-220 cm, and no significant difference in SIC stock at 220-300 cm was observed between the two lands (Fig. 6). The vertical distributions of SIC stock along the profile of 300 cm between the two lands were remarkably different. Under the forestland, the SIC stock was the lowest at 0-20 cm and the highest at 140-160 cm, and it increased gradually from 0 to 160 cm, decreased from 160 to 220 cm, and was evenly distributed

below 220 cm. Under the cropland, the SIC stock was the lowest at 0-20 cm and the highest at 40-60 cm, and it increased gradually from 0 to 60 cm, declined from 60 to 100 cm, and was evenly distributed within 100-300 cm layers (Fig. 6).

The PIC stock within the 0-300 cm depth under the forestland was 441.2 Mg ha^{-1}, which was significantly higher than that under the cropland (350.9 Mg ha^{-1}). Compared to cropland, the PIC stocks under the forestland were significantly lower at 0-80 cm but were dramatically higher at 80-300 cm (Fig. 7). The vertical distribution of PIC stock under the forestland showed an increasing trend from 0 to 160 cm and a decreasing trend from 160 to 220 cm; no significant difference in PIC stock was found among the 220-300 cm layers (Fig. 7). The vertical distribution of PIC stock under the cropland showed an increasing trend from 0 to 60 cm and a decreasing trend from 60 to 180 cm; no significant difference in PIC stock was found among the 180-300 cm layers (Fig. 7). At each soil layer, the LIC stock under the

Table 1 Soil bulk densities and soil pH under the cropland and forestland. Within each depth, different lowercase letters denote significant differences between the land-uses (mean ± standard deviation; n = 9; significance of the difference was considered as $P < 0.05$)

Depth (cm)	Bulk density (g cm^{-3})		pH	
	Forestland	Cropland	Forestland	Cropland
0-20	0.99 (0.08)b	1.08 (0.09)a	7.3 (0.2)b	7.8 (0.1)a
20-40	1.05 (0.08)b	1.22 (0.11)a	7.4 (0.2)b	8.1 (0.1)a
40-60	1.12 (0.08)b	1.27 (0.08)a	7.6 (0.1)b	8.2 (0.2)a
60-80	1.15 (0.06)b	1.23 (0.10)a	7.4 (0.3)b	8.3 (0.1)a
80-100	1.17 (0.07)a	1.19 (0.08)a	7.8 (0.2)b	8.3 (0.2)a
100-120	1.18 (0.04)a	1.19 (0.07)a	7.7 (0.1)b	8.4 (0.1)a
120-140	1.21 (0.06)a	1.19 (0.08)a	7.9 (0.1)b	8.2 (0.1)a
140-160	1.20 (0.09)a	1.18 (0.09)a	8.0 (0.2)b	8.3 (0.1)a
160-180	1.21 (0.08)a	1.20 (0.14)a	8.2 (0.2)a	8.1 (0.2)a
180-200	1.20 (0.09)a	1.17 (0.11)a	8.1 (0.2)a	8.2 (0.2)a
200-220	1.19 (0.07)a	1.19 (0.13)a	8.2 (0.2)a	8.0 (0.2)a
220-240	1.20 (0.05)a	1.17 (0.10)a	8.3 (0.1)a	8.1 (0.3)a
240-260	1.16 (0.06)a	1.18 (0.10)a	8.1 (0.1)a	8.2 (0.1)a
260-280	1.17 (0.09)a	1.19 (0.10)a	8.2 (0.2)a	7.9 (0.2)a
280-300	1.17 (0.08)a	1.17 (0.11)a	8.0 (0.1)a	8.1 (0.1)a

forestland was remarkably lower than that under the cropland (Fig. 8). The LIC stocks at 0-300 cm under the forestland and cropland were 195.0 Mg ha^{-1} and 292.2 Mg ha^{-1}, respectively, and the forestland stored significantly less LIC than the cropland within the 300 cm depth. The LIC stocks showed a roughly increasing trend from 0 to 300 cm under both forestland and cropland. Notably, in the 80-220 cm layer where the SIC stock under the forestland was significantly higher than the cropland, the LIC stock under the forestland was 41.1 Mg ha^{-1} lower than the cropland, while the PIC stock under the forestland was 98.9 Mg ha^{-1} higher than the cropland (Figs. 7, 8).

Discussion

The reduction of SIC within the upper layers following afforestation

We found that the SIC stock significantly decreased within the top 80 cm after afforestation on cropland (Fig. 6). Similar results were observed in previous studies on the CLP (Tan et al. 2014; Wang et al. 2016; An et al. 2019; Jia et al. 2019; Song et al. 2020), which reported that afforestation on cropland reduced SIC in the upper layers. It is widely accepted that afforestation on cropland strongly enhances soil and water conservation (Guo and Shao 2013), implying that the reduced SIC following afforestation should
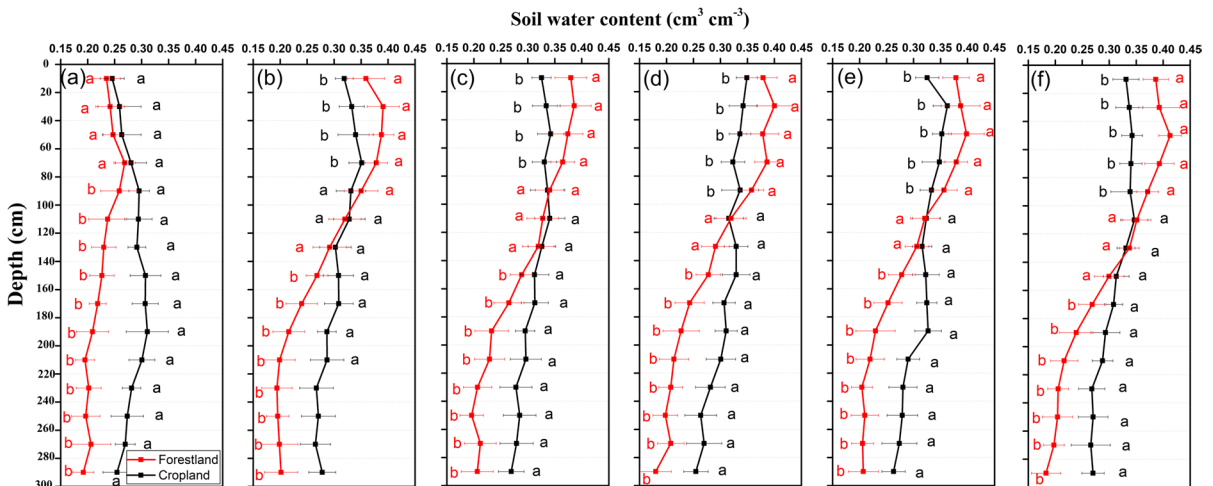

Fig. 3 Soil water contents under the forestland and cropland 48 hours after the rainfall. (**a**) was the soil water contents with no rainfall occurring; (**b**) to (**f**) were the soil water contents after the first, the second, the third, the fourth and the fifth from May to October 2018, respectively. Within each depth, different lowercase letters denote significant differences between the land-uses (mean ± standard deviations; n = 9; significance of the difference was considered as $P < 0.05$)
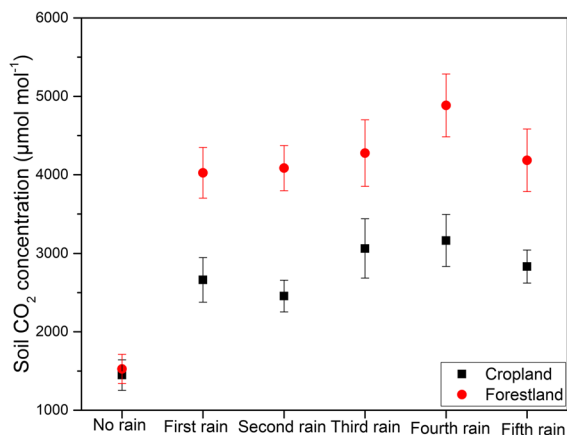
Fig. 4 Soil CO_2 concentrations at 50 cm depth under the forestland and cropland 48 hours after the rainfall. Within each depth, different lowercase letters denote significant differences between the land-uses (mean ± standard deviations; n = 9; significance of the difference was considered as $P < 0.05$)

not be carried in runoff from the forestry ecosystem by soil erosion. The reduction of SIC in the upper layers following afforestation may be related to the dissolution of carbonate induced by soil acidification (Chang et al. 2012; Han et al. 2018).

The dissolution of CO_2 from soil respiration would promote soil acidification in upper layers of forestland (Zamanian et al. 2018). The SWC in upper layers following rainfall under the forestland were significantly higher than the cropland in this study (Fig. 3), which was attributed to the stronger water infiltration in the forestland (Wang et al. 2015; Jia et al. 2017). The higher soil moisture motivates the activity of microorganisms (Tamir et al. 2012; Jia et al. 2013, 2018). As the main substrate of microbial decomposition, the SOC contents in topsoil of forestland were significantly higher than those under cropland (Fig. 2b). The stronger activity of microorganisms and richer SOC in the upper layers under the forestland enhanced the soil respiration, increased the soil CO_2 concentration (Fig. 4) and elevated the soil biogenic CO_2 partial pressures. The higher soil biogenic CO_2 partial
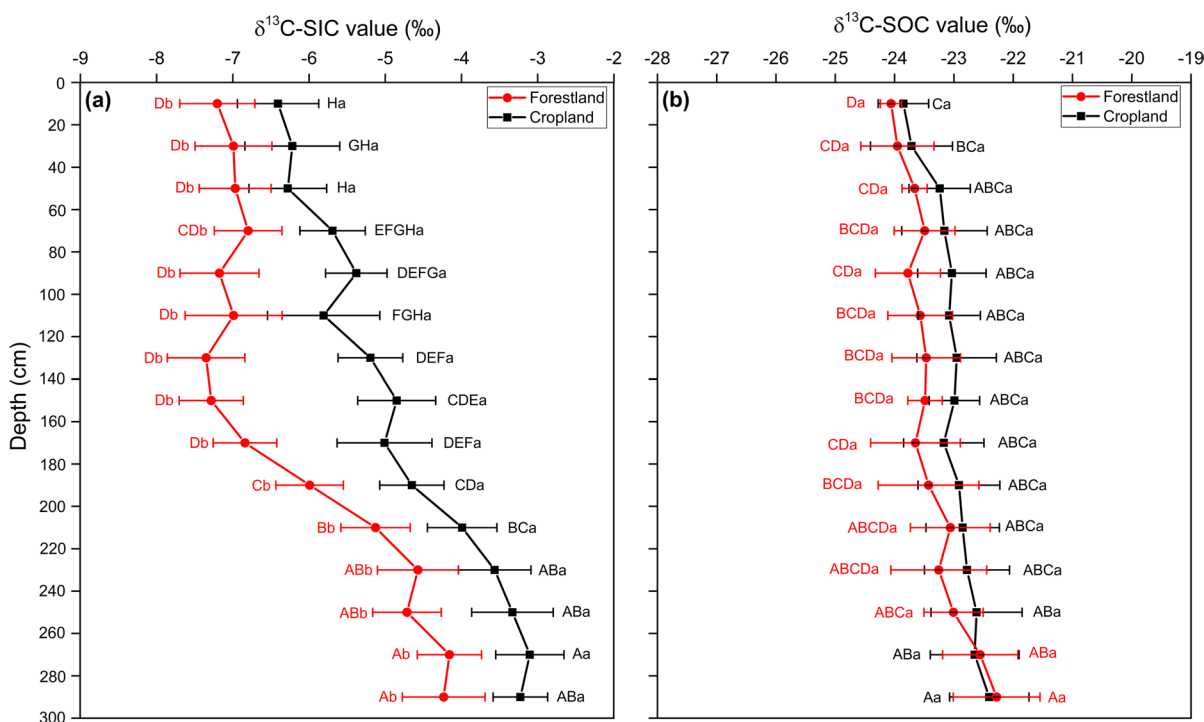

Fig. 5 δ^{13}C-SIC values and δ^{13}C-SOC values under forestland and cropland. Within each land-use, different uppercase letters denote significant differences among the depths, and within

each depth, different lowercase letters denote significant differences between the land-uses (mean ± standard deviations; n = 9; significance of the difference was considered as $P < 0.05$)
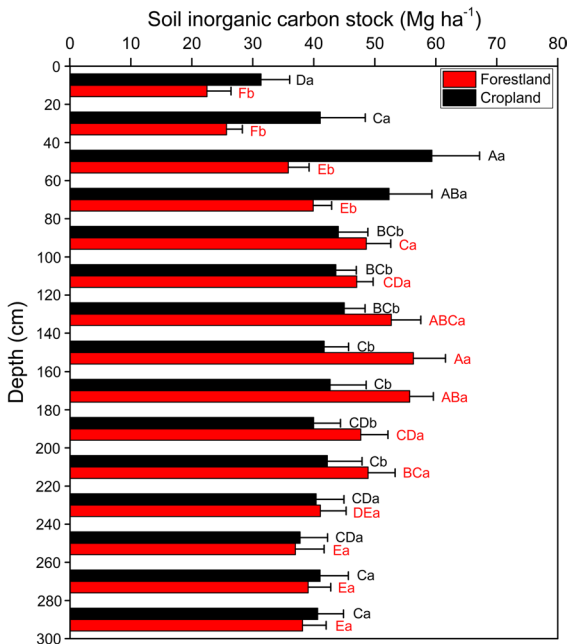
Fig. 6 Soil inorganic carbon stocks under forestland and cropland. Within each land-use, different uppercase letters denote significant differences among the depths, and within each depth, different lowercase letters denote significant differences between the land-uses (mean ± standard deviations; n = 9; significance of the difference was considered as $P < 0.05$)
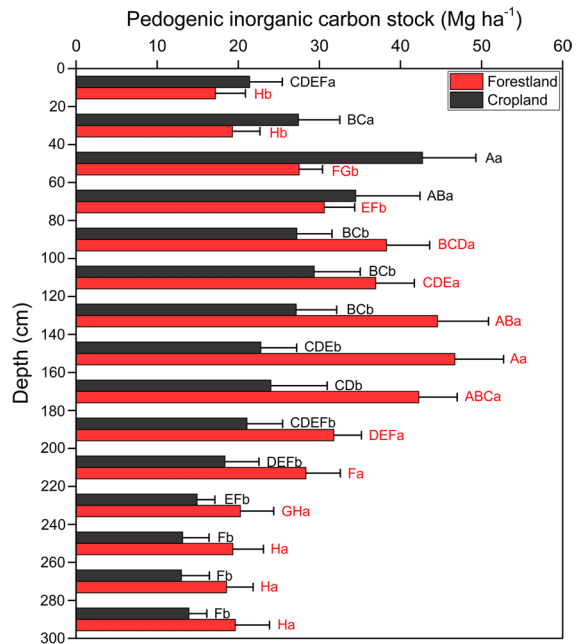
Fig. 7 Pedogenic inorganic carbon stocks under forestland and cropland. Within each land-use, different uppercase letters denote significant differences among the depths, and within each depth, different lowercase letters denote significant differences between the land-uses (mean ± standard deviations; n = 9; significance of the difference was considered as $P < 0.05$)
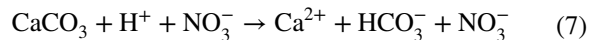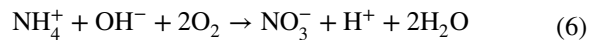
pressures and higher SWC (which can supply more water) would promote the dissolution of carbonate in the topsoil under the forestland (Eq. 5 is shifted to the right) (Zamanian et al. 2018):

$$CaCO_3 + CO_2 + H_2O \leftrightarrow CaCO_3 + H^+ + HCO_3^- \leftrightarrow Ca^{2+} + 2HCO_3^- \quad (5)$$
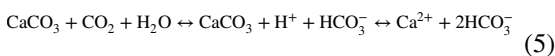
Due to the $\delta^{13}C$ value of the carbonate far exceeding that of biogenic CO_2 (Wang et al. 2014), the biogenic CO_2 participating in carbonate dissolution was supported by the decrease in $\delta^{13}C$-SIC at 0-80 cm following afforestation in this study (Fig. 5a). The percentage of dissolved CO_2 for the total respired CO_2 was considerable. In the calcareous soils of the northeast USA, up to 43% of respired CO_2 was potentially dissolved rather than directly diffusing out to the atmosphere (Hodges et al. 2021).

Furthermore, the nitrification of NH_4^+ coming from N_2 fixation by legumes and microbes would lead to topsoil acidification in forestland (Raza et al. 2020). As a typical legume, *R. pseudoacacia* with microbes has the ability to fix nitrogen by converting

N_2 to NH_4^+. In topsoil of dryland, part of NH_4^+ was oxidized to NO_3^- in the alkaline environment of sufficient oxygen, and much H^+ was released in this process (Eq. 6). In calcareous soils, the H^+ induced via nitrification of NH_4^+ would cause soil acidification and carbonate dissolution (Eq. 7; Huang et al. 2015):

$$NH_4^+ + OH^- + 2O_2 \rightarrow NO_3^- + H^+ + 2H_2O \quad (6)$$

$$CaCO_3 + H^+ + NO_3^- \rightarrow Ca^{2+} + HCO_3^- + NO_3^- \quad (7)$$

After carbonate dissolution, part of the carbon in SIC was conserved in the aqueous phase as HCO_3^- and formed dissolved inorganic carbon (DIC); part of the carbon in SIC was emitted into the atmosphere in the form of CO_2, and available NO_3^- and base cations (Ca^{2+}, Mg^{2+}) were released (Zamanian et al. 2018; Raza et al. 2020). When rainfall was occurring, the formed DIC, available NO_3^- and base cations in the upper layers would be leached into the deep layers with the infiltrated water (Mi et al. 2008; Ferdush and Paul 2021). Therefore, the reduction
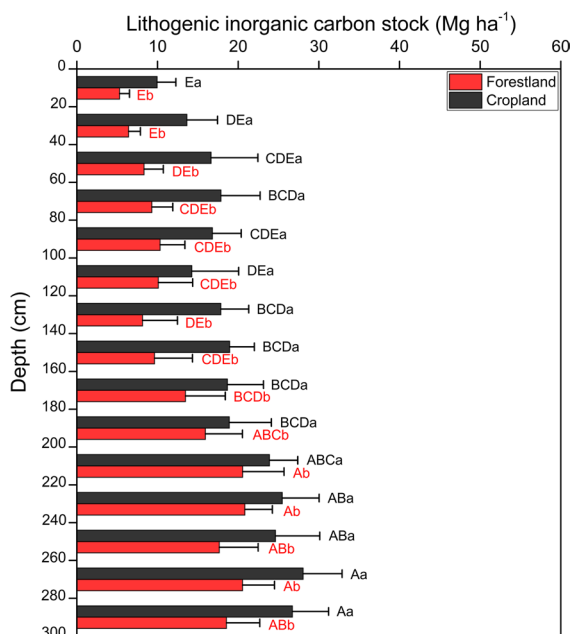
Fig. 8 Lithogenic inorganic carbon stocks under forestland and cropland. Within each land-use, different uppercase letters denote significant differences among the depths, and within each depth, different lowercase letters denote significant differences between the land-uses (mean ± standard deviations; n = 9; significance of the difference was considered as $P < 0.05$)

of SIC in the upper layers under the forestland was resulted from carbonate dissolution and the subsequent leaching of DIC and the emission of CO_2 from topsoil (Fig. 9).

The accumulation of PIC in the deep layers following afforestation

In this study, the SIC stock significantly increased at 80-220 cm following afforestation (Fig. 6). Han et al. (2018) and Jia et al. (2019) also found that the SIC stock increased in the deep layers (> 1 m) after afforestation on cropland on the CLP. In the 80-220 cm layer, the PIC stock under the forestland was 98.9 Mg ha^{-1} higher than that under the cropland (Fig. 7), indicating that afforestation on cropland considerably promotes PIC accumulation in deep layers. However, the LIC stock at 80-220 cm decreased by 41.1 Mg ha^{-1} (Fig. 8). The changes in PIC and LIC stocks at 80-220 cm following afforestation suggested that the increase in SIC within this layer was caused by the accumulation of PIC rather than the variation

of LIC. Notably, the δ^{13}C-LIC value for loess soil ranges from the minimum value at −2‰ to the maximum value at 0 on the CLP (Rao et al. 2006). When setting the δ^{13}C-LIC values as −2‰, −1‰ and 0 in this study, the PIC stocks at 0-300 cm under the forestland increased by 101.1 Mg ha^{-1}, 90.3 Mg ha^{-1} and 81.4 Mg ha^{-1}, respectively (Table 2). The maximum difference among the three values was 19.7 Mg ha^{-1}, which was very close to the standard deviations of the PIC stocks at 0-300 cm at the study site (Table 2). Therefore, based on Liu et al. (2011) and Wang et al. (2014), setting the δ^{13}C-LIC value as −1‰ is appropriate in the calculations of PIC stock in this study. Because conventional tillage only slightly declined the δ^{13}C-SOC value at 0-10 cm under the cropland and did not alter the δ^{13}C-SOC value below this depth (Ramnarine et al. 2012), the slight variation of δ^{13}C-SOC at 0-10 cm would not affect the calculations of PIC stock along the profile of 0-300 cm in this study.

There are a total of three mechanisms, which can induce the formation and accumulation of PIC in semiarid areas: (1) without the newly added Ca^{2+} or Mg^{2+}, the dissolution and precipitation of carbonate alternately occurs in situ with fluctuating dry-wet conditions (Eq. 5 is firstly shifted to the right due to the increasing of H_2O, and then is shifted to the left due to the declining of H_2O) (Chang et al. 2012; Wang et al. 2016; Sun et al. 2018); (2) after the dissolution of carbonate, the dissolved carbonate is transported in a dry environment and precipitates as PIC (Eq. 5 is shifted to the left due to the declining of H_2O) (Monger et al. 2015; Zamanian et al. 2016); (3) the added new Ca^{2+} or Mg^{2+}, which may be derived from deep groundwater, rainwater, irrigated water or fertilizer, combines with HCO_3^- and generates PIC in the alkaline environment (Eq. 5 is shifted to the left due to the increasing of Ca^{2+}) (Chang et al. 2012; Bughio et al. 2016; Gao et al. 2018). Obviously, the above three mechanisms are closely related to the soil water in deep layers. When no rainfall occurred, the SWC in the deep layers (>1 m) under forestland were much lower than cropland due to the strong transpiration of trees (Jia et al. 2017; Huang et al. 2020). After rainfall, the rainwater gradually infiltrated into the deep soil layers. The results of SWC following heavy rain in this study showed that when the rainwater reached the dry deep (1-2 m) layers in the forestland, it was
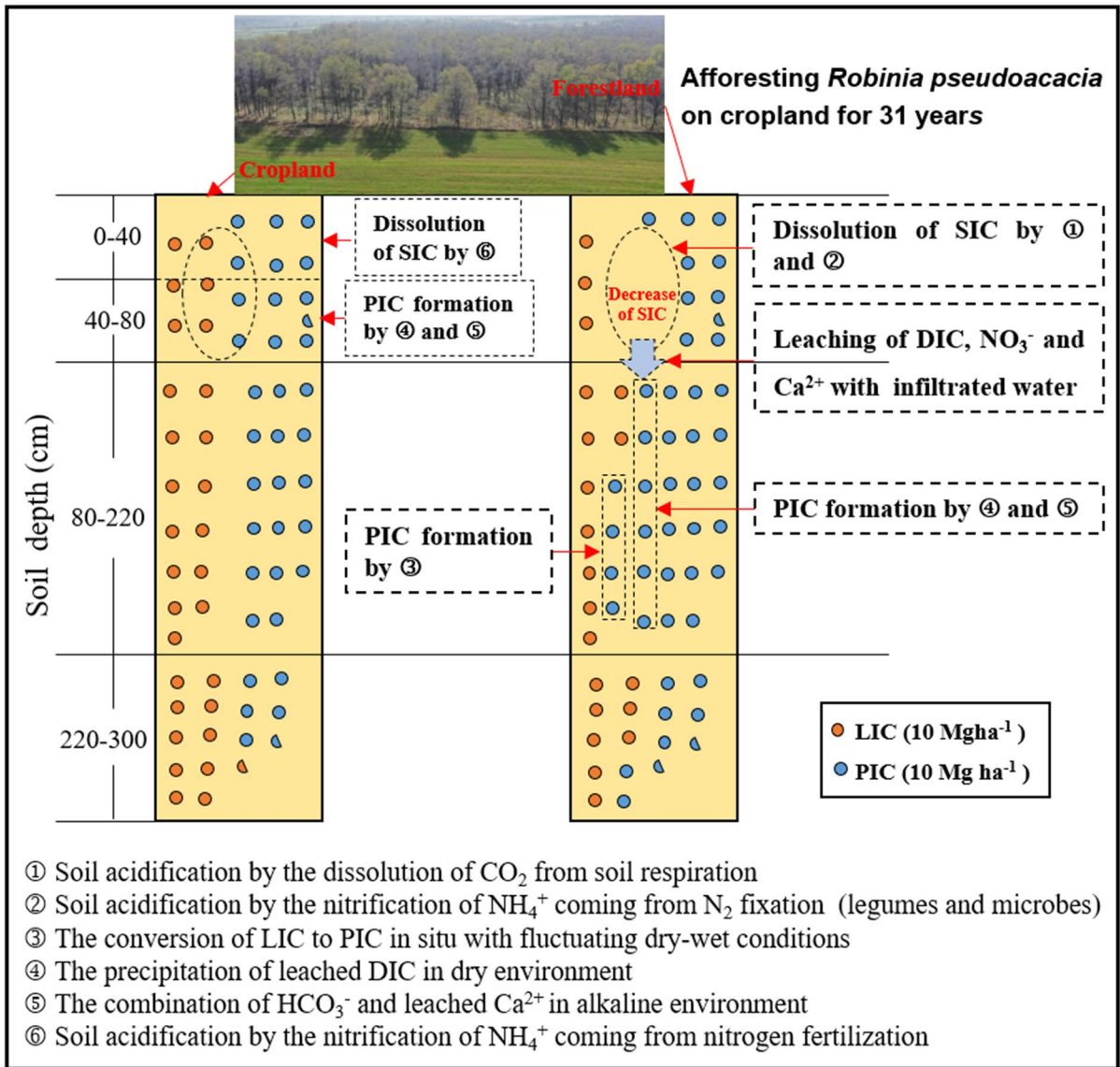
Fig. 9 Graphical representations of the dissolution, translocation and precipitation of soil inorganic carbon after afforestation on cropland (soil inorganic carbon, SIC; dissolved inorganic carbon, DIC; pedogenic inorganic carbon, PIC; lithogenic inorganic carbon, LIC)

absorbed and intercepted in these layers and was difficult to further move into the deeper (>2 m) layers (Fig. 3). The percolated water reached by deep (1-2 m) layers was lost by strong transpiration of trees, and the soil at these layers gradually became dry again. In this study, the formation and accumulation of PIC were significantly affected by the percolated solution from the upper soil layers.

After rainfall, the percolated water from the upper soil layers arrived at the dry layers and significantly increased the SWC in the deep layers. Similar with the carbonate dissolution in the upper layers, the rising SWC (which motivates the activity of microorganisms) and the higher SOC contents (Fig. 2b) (which can supply more substrate for microbial decomposition) promote the dissolution of carbonate in deep layers under the forestland. Furthermore, the nitrification

Table 2 Pedogenic inorganic carbon stocks (Mg ha^{-1}) when setting δ^{13}C-LIC values as −2‰, −1‰ and 0

Depth (cm)	−2.00‰		−1.00‰		0.00‰	
	Forestland	Cropland	Forestland	Cropland	Forestland	Cropland
0-20	19.6 (4.2)	24.5 (4.7)	17.2 (3.7)	21.4 (4.0)	15.3 (3.3)	19.0 (3.5)
20-40	22.1 (4.0)	31.5 (6.0)	19.3 (3.4)	27.4 (5.1)	17.1 (3.0)	24.3 (4.5)
40-60	31.6 (3.2)	49.5 (7.7)	27.5 (2.9)	42.7 (6.6)	24.4 (2.6)	37.6 (5.8)
60-80	35.3 (4.4)	40.2 (9.7)	30.6 (3.8)	34.5 (7.9)	27.0 (3.3)	30.2 (6.7)
80-100	43.9 (6.2)	31.7 (5.2)	38.3 (5.3)	27.2 (4.3)	33.9 (4.7)	23.8 (3.7)
100-120	42.6 (5.9)	34.2 (7.0)	37.0 (4.8)	29.4 (5.7)	32.7 (4.0)	25.7 (4.8)
120-140	51.5 (7.6)	31.8 (6.2)	44.6 (6.3)	27.1 (5.0)	39.3 (5.4)	23.7 (4.2)
140-160	53.8 (7.0)	26.6 (5.3)	46.7 (6.0)	22.8 (4.4)	41.3 (5.3)	19.9 (3.8)
160-180	48.7 (6.0)	28.0 (8.4)	42.3 (4.7)	24.0 (7.0)	37.4 (3.9)	21.1 (5.9)
180-200	36.8 (4.2)	24.7 (5.5)	31.8 (3.4)	21.1 (4.4)	28.0 (2.9)	18.4 (3.6)
200-220	33.0 (5.2)	21.5 (5.0)	28.4 (4.2)	18.4 (4.2)	24.8 (3.6)	16.0 (3.6)
220-240	23.5 (4.9)	17.5 (2.6)	20.3 (4.1)	14.9 (2.2)	17.8 (3.6)	13.0 (1.9)
240-260	22.5 (4.5)	15.5 (4.0)	19.3 (3.8)	13.1 (3.3)	16.9 (3.2)	11.4 (2.8)
260-280	21.9 (4.0)	15.3 (4.3)	18.5 (3.3)	13.0 (3.5)	16.1 (2.8)	11.3 (2.9)
280-300	23.4 (5.5)	16.5 (2.9)	19.6 (4.2)	13.9 (2.2)	16.9 (3.4)	12.0 (1.8)
0-300	510.1 (24.3)	409.0 (46.1)	441.3 (20.6)	351.0 (37.6)	388.9 (17.9)	307.5 (31.7)

of NH$_4^+$ in deep layers could add acidity to the subsoil and increase the carbonate dissolution regardless of weak nitrification due to low oxygen concentration in deep layers (Eq. 6). In the above two processes, both LIC and PIC were dissolved. After LIC dissolution, the dissolved LIC precipitated in situ as PIC with the decrease in SWC in the deep layers (mechanism (1)). Similarly, mechanism (1) should also occur in the topsoil of the forestland, which was supported by the declining of δ^{13}C-SIC (Fig. 4a) and the reduction of LIC in these layers (Fig. 8). In this study, the LIC stock within 80-220 cm decreased by 41.1 Mg ha^{-1} after afforestation (Fig. 8), and the amount of increased PIC through mechanism (1) accounted for only 41.6% of the total increased PIC at 80-220 cm, suggesting that the other two mechanisms may play an important role in the increase of PIC in this layer.

After the percolated solution from the upper soil layers reached the deep layers, the DIC carried in the percolated water would rapidly precipitate in the form of PIC in the dry environment (Zamanian et al. 2016; Ferdush and Paul 2021), resulting in the accumulation of PIC (mechanism (2)). Meanwhile, the available NO$_3^-$ and base cations carried in the percolated water also affected the formation of PIC in the deep layers. As the available NO$_3^-$ being assimilated by the deep roots of *R. pseudoacacia* (a typical nitrate-philic plant), the base cations from the upper layers

remained in the deep layers, which added new base cations in these layers. In the alkaline environment (Table 1), the newly added base cations combined with HCO$_3^-$ and generated PIC, causing the accumulation of PIC (mechanism (3)). Additionally, the results showed that no significant difference in SIC stock between forestland and cropland was found at 220-300 cm in this study (Fig. 6), which may be attributed to little solutes in percolated solution arriving >220 cm depth in the forestland (Fig. 3) and the weaker root activity below these depths.

Overall, the accumulation of PIC in the deep layers following afforestation was codetermined by the above three mechanisms. Because mechanism (1) only converted LIC into PIC in situ and did not alter the SIC stock, the net increases in PIC and SIC in the deep layers following afforestation were attributed to mechanism (2) and mechanism (3) (Fig. 9). However, the relative contributions of mechanism (2) and mechanism (3) to PIC accumulation should be explored in future studies. It should be noted that, the ions in the rainwater and in the atmospheric deposition of wind-blown calcareous dust could add Ca^{2+} and induce PIC accumulation (Mikhailova et al. 2020). Because the neighbouring forestland and cropland always receive the same amount of ions from the rainfall and the same amount of calcareous dust, the two processes would not cause the difference in

PIC stock between the two lands. Nevertheless, the detailed amounts of accumulated PIC via Ca^{2+} additions from rainfall and atmospheric deposition should be identified in future studies. Additionally, nitrogen fertilization could induce topsoil acidification and carbonate dissolution in the croplands of this study due to the nitrification of NH_4^+. After carbonate dissolution, available NO_3^- and Ca^{2+} were released, and part of the SIC was converted into DIC. The DIC and available NO_3^- and Ca^{2+} in the topsoil could be leached into the subsoil and form PIC (Fig. 9), resulting in a higher PIC stock at 40-80 cm than at 0-40 cm in the cropland in this study.

Changes in SIC along the profile following afforestation and its effects on soil fertility and soil carbon budget

We found that afforestation on cropland induced the dissolution of carbonate and the reduction of SIC in the upper layers. The presence of carbonate in the soil is essential to soil fertility and ecosystem functions (Raza et al. 2020). The dissolution of SIC has the following negative consequences: decreasing soil buffering capacity and resulting in the leaching of base cations (Lucas et al. 2011); decreasing the stability of soil aggregates and causing poor structure of the soil (Fernández-Ugalde et al. 2014); decreasing soil pH and affecting the availability of nutrients, microbial activity and community structure (Rousk et al. 2010). Importantly, carbonate dissolution in the upper layers increased the soil CO_2 efflux and represented a significant potential source of CO_2 to the atmosphere. Based on a global nitrogen fertilization map and the distribution of SIC within the 0-100 cm depth, the annual amount of soil CO_2 emissions induced by nitrogen fertilization was 7.48×10^{12} g C (Zamanian et al. 2018). The proportion of CO_2 originating from carbonate dissolution within the 0-50 cm layers occupied more than half of the total emitted CO_2 in Canada (Ramnarine et al. 2012). Over the past 40 years, the annual CO_2 efflux from the top 40 cm soil was tremendous in Chinese croplands due to $CaCO_3$ dissolution by nitrogen fertilization (Raza et al. 2020). The dramatic loss of SIC in the topsoil following nitrogen fertilization sparked heightened concerns, while not enough attention was given to the variations in SIC and PIC in deep layers.

In this study, afforestation on cropland considerably promoted PIC accumulation in the deep layers, and no significant difference in total SIC stock at 0-300 cm was observed between the two lands. The net increased PIC at 80-220 cm (57.8 Mg ha^{-1}; Fig. 7) in the deep layers compensated for the loss of SIC in the upper layers (60.2 Mg ha^{-1}; Fig. 6), suggesting that there is no need to worry about the carbon in the SIC pool in the upper layers following afforestation being emitted into the atmosphere. Afforestation on cropland does not alter the total SIC storage but redistributes the SIC along the profile on the CLP. Our results also implied that when exploring the effects of land-use change or cultivation on the SIC in drylands, particular attention should be given to the changes in PIC along the profile, especially in deep layers. Neglecting this information could misestimate the carbon budget in these lands.

Conclusions

The results demonstrated that, afforestation on cropland reduces the SIC in the upper layers, which is resulted from the dissolution of carbonate. Afforestation on cropland promotes PIC accumulation in the deep layers, and the increase in SIC in these layers is caused by the accumulation of PIC. Because the net increased PIC in the deep layers compensates for the loss of SIC in the upper layers, afforestation on cropland does not alter the total SIC storage but redistributes the SIC along the profile on the CLP. Our findings highlight the importance of the variations in PIC in deep layers following land-use change in drylands.

References

An H, Wu XZ, Zhang YR, Tang ZS (2019) Effects of land-use change on soil inorganic carbon: a meta-analysis. Geoderma 353:273–282. https://doi.org/10.1016/j.geoderma.2019.07.008

Belay-Tedla A, Zhou XH, Su B, Wan SQ, Luo YQ (2009) Labile, recalcitrant, and microbial carbon and nitrogen pools of a tallgrass prairie soil in the US Great Plains subjected to experimental warming and clipping. Soil Biol Biochem 41:110–116. https://doi.org/10.1016/j.soilbio.2008.10.003

Bughio MA, Wang PL, Meng FQ, Qing C, Kuzyakov Y, Wang XJ, Junejo SA (2016) Neoformation of pedogenic carbonates by irrigation and fertilization and their contribution to carbon sequestration in soil. Geoderma 262:12–19. https://doi.org/10.1016/j.geoderma.2015.08.003

Cerling TE, Quade J, Wang Y, Bowman JR (1989) Carbon isotopes in soils and palaeosols as ecology and palaeoecology indicators. Nature 341:138–139. https://doi.org/10.1038/341138a0

Cerling TE, Solomon DK, Quade J, Bowman JR (1991) On the isotopic composition of carbon in soil carbon dioxide. Geochim Cosmochim Acta 55:3403–3405. https://doi.org/10.1016/0016-7037(91)90498-T

Chang RY, Fu BJ, Liu GH, Wang S, Yao XL (2012) The effects of afforestation on soil organic and inorganic carbon: a case study of the loess plateau of China. Catena 95:145–152. https://doi.org/10.1016/j.catena.2012.02.012

Deng L, Liu GB, Shangguan ZP (2014) Land-use conversion and changing soil carbon stocks in China's "grain-for-green" program: a synthesis. Glob Chang Biol 20:3544–3556. https://doi.org/10.1111/gcb.12508

Emmerich WE (2003) Carbon dioxide fluxes in a semiarid environment with high carbonate soils. Agric For Meteorol 116:91–102. https://doi.org/10.1016/S0168-1923(02)00231-9

Ferdush J, Paul V (2021) A review on the possible factors influencing soil inorganic carbon under elevated CO_2. Catena 204:105434. https://doi.org/10.1016/j.catena.2021.105434

Fernández-Ugalde O, Virto I, Barré P, Apesteguía M, Enrique A, Imaz MJ, Bescansa P (2014) Mechanisms of macroaggregate stabilisation by carbonates: implications for organic matter protection in semi-arid calcareous soils. Soil Res 52:180–192. https://doi.org/10.1071/SR13234

Gao Y, Tian J, Pang Y, Liu JB (2017) Soil inorganic carbon sequestration following afforestation is probably induced by Pedogenic carbonate formation in Northwest China. Front Plant Sci 8:1282. https://doi.org/10.3389/fpls.2017.01282

Gao Y, Dang P, Zhao QX, Liu JL, Liu JB (2018) Effects of vegetation rehabilitation on soil organic and inorganic carbon stocks in the mu Us Desert, Northwest China. Land Degrad Dev 29:1031–1040. https://doi.org/10.1002/ldr.2832

Guo Z, Shao M (2013) Impact of afforestation density on soil and water conservation of the semiarid loess plateau, China. J Soil Water Conserv 68:401–410. https://doi.org/10.2489/jswc.68.5.401

Han XY, Gao GY, Chang RY, Li ZS, Ma Y, Wang S, Wang C, Lu YH, Fu BJ (2018) Changes in soil organic and inorganic carbon stocks in deep profiles following cropland abandonment along a precipitation gradient across the loess plateau of China. Agric Ecosyst Environ 258:1–13. https://doi.org/10.1016/j.agee.2018.02.006

He SX, Liang ZS, Han RL, Wang Y, Liu GB (2016) Soil carbon dynamics during grass restoration on abandoned sloping cropland in the hilly area of the loess plateau, China. Catena 137:679–685. https://doi.org/10.1016/j.catena.2015.01.027

Hodges C, Brantley SL, Sharifironizi M, Forsythe B, Tang Q, Carpenter N, Kaye J (2021) Soil carbon dioxide flux partitioning in a calcareous watershed with agricultural impacts. J Geophys Res Biogeosci 126:e2021JG006379. https://doi.org/10.1029/2021JG006379

Huang P, Zhang JB, Xin XL, Zhu AN, Zhang CZ, Zhu QG, Ma DH, Zhu QG, Yang S, Wu SJ (2015) Proton accumulation accelerated by heavy chemical nitrogen fertilization and its long-term impact on acidifying rate in a typical arable soil in the Huang-Huai-Hai plain. J Integr Agric 14:148–157. https://doi.org/10.1016/S2095-3119(14)60750-4

Huang Z, Yang WJ, Liu Y, Shen WB, López-Vicente M, Wu GL (2020) Belowground soil water response in the afforestation-cropland interface under semi-arid conditions. Catena 193:104660. https://doi.org/10.1016/j.catena.2020.104660

Jackson RB, Banner JL, Jobbágy EG, Pockman WT, Wall DH (2002) Ecosystem carbon loss with woody plant invasion of grasslands. Nature 418:623–626. https://doi.org/10.1038/nature00910

Jia X, Zha TS, Wu B, Zhang YQ, Chen WJ, Wang XP, Yu HQ, He GM (2013) Temperature response of soil respiration in a Chinese pine plantation: hysteresis and seasonal vs. diel Q10. PLoS One 8:e57858. https://doi.org/10.1371/journal.pone.0057858

Jia XX, Shao MA, Zhu YJ, Luo Y (2017) Soil moisture decline due to afforestation across the loess plateau, China. J Hydrol 546:113–122. https://doi.org/10.1016/j.jhydrol.2017.01.011

Jia X, Zha TS, Wang S, Bourque CPA, Wang B, Qin SG, Zhang YQ (2018) Canopy photosynthesis modulates soil respiration in a temperate semi-arid shrubland at multiple timescales. Plant Soil 432:437–450. https://doi.org/10.1007/s11104-018-3818-z

Jia XX, Wang X, Hou LC, Wei XR, Zhang Y, Shao MA, Zhao XN (2019) Variable response of inorganic carbon and consistent increase of organic carbon as a consequence of afforestation in areas with semiarid soils. Land Degrad Dev 30:1345–1356. https://doi.org/10.1002/ldr.3320

Jin Z, Dong YS, Wang YQ, Wei XR, Wang YF, Cui BL, Zhou WJ (2014) Natural vegetation restoration is more beneficial to soil surface organic and inorganic carbon sequestration than tree plantation on the loess plateau of China.

Sci Total Environ 485–486:615–623. https://doi.org/10.1016/j.scitotenv.2014.03.105

Lal R (2004) Soil carbon sequestration impacts on global climate change and food security. Science 304:1623–1627. https://doi.org/10.1126/science.1097396

Lal R (2009) Sequestering carbon in soils of arid ecosystems. Land Degrad Dev 20:441–454. https://doi.org/10.1002/ldr.934

Landi A, Mermut AR, Anderson DW (2003) Origin and rate of pedogenic carbonate accumulation in Saskatchewan soils, Canada. Geoderma 117:143–156. https://doi.org/10.1016/S0016-7061(03)00161-7

Liu WG, Yang H, Sun YB, Wang XL (2011) $\delta^{13}C$ values of loess total carbonate: a sensitive proxy for Asian summer monsoon in arid northwestern margin of the Chinese loess plateau. Chem Geol 284:317–322. https://doi.org/10.1016/j.chemgeo.2011.03.011

Lucas RW, Klaminder J, Futter MN, Bishop KH, Egnell G, Laudon H, Högberg P (2011) A meta-analysis of the effects of nitrogen additions on base cations: implications for plants, soils, and streams. For Ecol Manag 262:95–104. https://doi.org/10.1016/j.foreco.2011.03.018

Mermut AR, Amundson R, Cerling TE (2000) The use of stable isotopes in studying carbonate dynamics in soils. In: Lal R, Kimble JM, Eswaran H, Stewart BA (eds) Global climate change and pedogenic carbonates. CRC Press, Boca Raton

Mi N, Wang SQ, Liu JY, Yu GR, Zhang WJ, Jobbágy E (2008) Soil inorganic carbon storage pattern in China. Glob Chang Biol 14:2380–2387. https://doi.org/10.1111/j.1365-2486.2008.01642.x

Mikhailova EA, Zurqani HA, Post CJ, Schlautman MA (2020) Assessing ecosystem services of atmospheric calcium and magnesium deposition for potential soil inorganic carbon sequestration. Geosciences 10:200. https://doi.org/10.3390/geosciences10050200

Monger HC, Kraimer RA, Khresat S, Cole DR, Wang X, Wang J (2015) Sequestration of inorganic carbon in soil and groundwater. Geology 43:375–378. https://doi.org/10.1130/G36449.1

Ramnarine R, Wagner-Riddle C, Dunfield KE, Voroney RP (2012) Contributions of carbonates to soil CO_2 emissions. Can J Soil Sci 92:599–607. https://doi.org/10.4141/CJSS2011-025

Rao ZG, Zhu ZY, Chen FH, Zhang JW (2006) Does $\delta^{13}C_{carb}$ of the Chinese loess indicate past C_3/C_4 abundance? A review of research on stable carbon isotopes of the Chinese loess. Quat Sci Rev 25:2251–2257. https://doi.org/10.1016/j.quascirev.2006.03.013

Raza S, Miao N, Wang PZ, Ju XT, Chen ZJ, Zhou JB, Kuzyakov Y (2020) Dramatic loss of inorganic carbon by nitrogen-induced soil acidification in Chinese croplands. Glob Chang Biol 26:3738–3751. https://doi.org/10.1111/gcb.15101

Rousk J, Bååth E, Brookes PC, Lauber CL, Lozupone C, Caporaso JG, Knight R, Fierer N (2010) Soil bacterial and fungal communities across a pH gradient in an arable soil. ISME J 4:1340–1351. https://doi.org/10.1038/ismej.2010.58

Ryskov YG, Demkin VA, Oleynik SA, Ryskova EA (2008) Dynamics of pedogenic carbonate for the last 5000 years and its role as a buffer reservoir for atmospheric carbon

dioxide in soils of Russia. Glob Planet Chang 61:63–69. https://doi.org/10.1016/j.gloplacha.2007.08.006

Schlesinger WH (1982) Carbon storage in the caliche of arid soils: a case study from Arizona. Soil Sci 133:247–255. https://doi.org/10.1097/00010694-198204000-00008

Schmidt MWI, Torn MS, Abiven S, Dittmar T, Guggenberger G, Janssens IA, Kleber M, Kögel-Knabner I, Lehmann J, Manning DAC, Nannipieri P, Rasse DP, Weiner S, Trumbore SE (2011) Persistence of soil organic matter as an ecosystem property. Nature 478:49–56. https://doi.org/10.1038/nature10386

Song Y, Yao YF, Qin X, Wei XR, Jia XX, Shao MA (2020) Response of carbon and nitrogen to afforestation from 0 to 5 m depth on two semiarid cropland soils with contrasting inorganic carbon concentrations. Geoderma 357:113940. https://doi.org/10.1016/j.geoderma.2019.113940

Stevenson BA, Kelly EF, McDonald EV, Busacca AJ (2005) The stable carbon isotope composition of soil organic carbon and pedogenic carbonates along a bioclimatic gradient in the Palouse region, Washington state, USA. Geoderma 124:37–47. https://doi.org/10.1016/j.geoderma.2004.03.006

Sun WH, Zhao XN, Ling Q, Li HC, Gao XD (2018) Revegetation modifies patterns of temporal soil respiration responses to extreme-drying-and-rewetting in a semiarid ecosystem. Plant Soil 433:227–241. https://doi.org/10.1007/s11104-018-3835-y

Tamir G, Shenker M, Heller H, Bloom PR, Fine P, Bar-Tal A (2012) Dissolution and re-crystallization processes of active calcium carbonate in soil developed on tufa. Soil Sci Soc Am J 76:1606–1613. https://doi.org/10.2136/sssaj2012.0041

Tan WF, Zhang R, Cao H, Huang CQ, Yang QK, Wang MK, Koopal LK (2014) Soil inorganic carbon stock under different soil types and land uses on the loess plateau region of China. Catena 121:22–30. https://doi.org/10.1016/j.catena.2014.04.014

von Caemmerer S, Ghannoum O, Pengelly JJL, Cousins AB (2014) Carbon isotope discrimination as a tool to explore C4 photosynthesis. J Exp Bot 65:3459–3470. https://doi.org/10.1093/jxb/eru127

Walkley AJ, Black IA (1934) An examination of the Degtjareff method for determining soil organic matter and a proposed modification of the chromic acid titration method. Soil Sci 37:29–38. https://doi.org/10.1097/00010694-19340 1000-00003

Wang XJ, Wang JP, Zhang J (2012) Comparisons of three methods for organic and inorganic carbon in calcareous soils of northwestern China. PLoS One 7:e44334. https://doi.org/10.1371/journal.pone.0044334

Wang XJ, Xu MG, Wang JP, Zhang WJ, Yang XY, Huang SM, Liu H (2014) Fertilization enhancing carbon sequestration as carbonate in arid cropland: assessments of long-term experiments in northern China. Plant Soil 380:89–100. https://doi.org/10.1007/s11104-014-2077-x

Wang L, Zhong CG, Gao PX, Xi WM, Zhang SX (2015) Soil infiltration characteristics in agroforestry systems and their relationships with the temporal distribution of rainfall on the loess plateau in China. PLoS One 10:e0124767. https://doi.org/10.1371/journal.pone.0124767

Wang KB, Ren ZP, Deng L, Zhou ZC, Shangguan ZP, Shi WY, Chen YP (2016) Profile distributions and controls of soil

inorganic carbon along a 150-year natural vegetation restoration chronosequence. Soil Sci Soc Am J 80:193–202. https://doi.org/10.2136/sssaj2015.08.0296

World Reference Base for Soil Resources (2014) International soil classification system for naming soils and creating legends for soil maps

Wu HB, Guo ZT, Gao Q, Peng CH (2009) Distribution of soil inorganic carbon storage and its changes due to agricultural land use activity in China. Agric Ecosyst Environ 129:413–421. https://doi.org/10.1016/j.agee.2008.10.020

Xiao W, Zhang WK, Ye YM, LV, XJ, Yang WF (2020) Is underground coal mining causing land degradation and significantly deteriorating ecosystems in arid areas? A perspective from ecological capital. Land Degrad Dev 31:1969–1989. https://doi.org/10.1002/ldr.3570

Yang LQ, Zhu GD, Ju XT, Liu R (2021) How nitrification-related N_2O is associated with ammonia oxidizers in two contrasting soils in China? Sci Total Environ 770:143212. https://doi.org/10.1016/j.scitotenv.2020.143212

Yu X, Zhou WJ, Chen YP, Wang YQ, Cheng P, Hou YY, Wang Y, Xiong XH, Yang L (2020) Spatial variation of soil properties and carbon under different land use types on the Chinese loess plateau. Sci Total Environ 703:134946. https://doi.org/10.1016/j.scitotenv.2019.134946

Zhang YJ, Guo SL, Liu QF, Jiang JS, Wang R, Li NN (2015) Responses of soil respiration to land use conversions in degraded ecosystem of the semi-arid loess plateau. Ecol Eng 74:196–205. https://doi.org/10.1016/j.ecoleng.2014.10.003

Zamanian K, Pustovoytov K, Kuzyakov Y (2016) Pedogenic carbonates: forms and formation processes. Earth-Sci Rev 157:1–17. https://doi.org/10.1016/j.earscirev.2016.03.003

Zamanian K, Mohsen Z, Kuzyakov Y (2018) Nitrogen fertilization raises CO_2 efflux from inorganic carbon: a global assessment. Glob Chang Biol 24:2810–2817. https://doi.org/10.1111/gcb.14148